Estimation of VTI parameters using slowness-polarization inversion of P- and SV-waves

Naser Tamimi*, I. Tsvankin † and Thomas L. Davis†

* *Sigma Cubed (SIGMA^3) Inc.* † *Department of Geophysics, Colorado School of Mines*

(August 11, 2015)

Running head: **Joint P and SV slowness-polarization**

ABSTRACT

Ignoring anisotropy may cause serious distortions in the results of seismic data processing and interpretation. Although P-wave data provide valuable information for estimating anisotropy parameters, important additional constraints can be obtained from shear waves. Here, we present an extension of the slowness-polarization method for VSP data, in which we combine the vertical slownesses and polarization angles of P- and SV-waves. The algorithm is developed for VTI (transversely isotropic with a vertical symmetry axis) media, but it can be generalized for azimuthally anisotropic models.

The weak-anisotropy approximation shows that adding SV-wave data generally stabilizes slowness-polarization inversion. In particular, SV-waves improve not only estimation of the anellipticity parameter η but also help constrain the coefficient δ, if propagation angles around 45° are available.

The proposed technique is applied to a synthetic VSP data set generated using a finite-difference code. This test confirms that including SV-waves yields better inversion results than those obtained solely from P-wave data.

INTRODUCTION

Including information about seismic anisotropy is essential for seismic processing, imaging, interpretation, and reservoir characterization. Ignoring anisotropy causes serious distortions, such as unfocused migrated images, misplaced reflectors, and incorrect amplitude recovery (e.g., Tsvankin and Grechka, 2011). One of the main difficulties in taking anisotropy into account is nonuniqueness of estimated anisotropy parameters.

Vertical seismic profiling (VSP) data can be used to determine local (in-situ) anisotropy with spatial resolution close to the dominant seismic wavelength (Tsvankin, 2012). Local estimation of the anisotropy parameters from traveltimes and polarizations recorded in boreholes is discussed in a number of publications (e.g., Miller and Spencer, 1994; Horne and Leaney, 2000; Dewangan and Grechka, 2003; Grechka and Mateeva, 2007; Grechka et al., 2007; Pevzner et al., 2011; Rusmanugroho and McMechan, 2012b,a). The majority of these techniques use the slowness and polarization vectors of transmitted (or direct) waves.

Because the horizontal slowness components are not preserved in the case of a laterally heterogeneous overburden, VSP data typically provide accurate estimates only of the vertical slowness. Valuable additional information can be obtained from the polarization vector, and if all slowness and polarization components are available, including polarizations makes the inversion for the stiffnesses linear (Dewangan and Grechka, 2003). Grechka and Mateeva (2007) develop an inversion algorithm for VTI media that combines the vertical slowness and polarization angle of P-waves.

Here, we first describe the theory of the slowness-polarization method. Then we modify the P-wave slowness-polarization technique of Grechka and Mateeva (2007) by including SV-wave data. The advantage of including SV-waves into the inversion is discussed by an-

alyzing the weak-anisotropy approximation for the slowness-polarization function. Finally, the modified method is applied to a synthetic VSP data set.

THEORY

Plane-wave propagation in anisotropic media is described by the Christoffel equation:

$$[G_{ik} - \rho V^2 \delta_{ik}]\, U_k = 0\,, \tag{1}$$

where ρ is the density, V is the phase velocity, δ_{ik} is Kronecker's delta, $\mathbf{U}$ is the polarization vector, and G_{ik} is the Christoffel matrix defined as:

$$G_{ik} = c_{ijkl} n_j n_l\,; \tag{2}$$

$\mathbf{n}$ is the unit slowness vector and c_{ijkl} are the stiffness coefficients. The eigenvalues of the Christoffel matrix are found from

$$\det[G_{ik} - \rho\, V^2 \delta_{ik}] = 0. \tag{3}$$

Solving eq. (3) yields three eigenvalues corresponding to the phase velocities of P-, S_1-, and S_2-waves (V_P, V_{S1}, and V_{S2}). Substituting each phase velocity into eq. (1) yields the corresponding eigenvector or polarization vector $\mathbf{U}$, which deviates from its direction in isotropic media. The slowness vector for each mode is defined as $\mathbf{p} = \mathbf{n}/V$.

VSP surveys with multicomponent geophones provide a unique opportunity to measure polarization vectors along with the slownesses. These measurements can be employed in

the inversion for the elements of the tensor c_{ijkl}, or the equivalent anisotropy parameters, in different ways (Tsvankin and Grechka, 2011). Below we review the slowness and slowness-polarization methods, which are most widely used in practice.

Slowness Method

Early publications on estimating local anisotropy from VSP data operated with the P-wave slowness vector (White et al., 1983; Gaiser, 1990; Miller and Spencer, 1994). The horizontal slownesses p_1 and p_2 can be approximately determined from common-receiver gathers, while the vertical slowness $q = p_3$ in vertical boreholes is estimated from common-source gathers (Gaiser, 1990):

$$p_{i,Q} = \partial t / \partial x_i, \qquad (i = 1, 2, 3; \quad Q = P, S_1, S_2). \tag{4}$$

Then eq. (3) is inverted for the stiffness coefficients at the receiver location using the available source locations. This inversion technique relies on the preservation of the horizontal slowness components in a laterally homogeneous medium (according to Snell's law) above the receiver. But this assumption is invalid in the presence of lateral heterogeneity, and the horizontal slownesses cannot be found directly from the data. There are several techniques designed to correct the horizontal slowness for lateral heterogeneity (e.g., Jílek et al., 2003), but they are difficult to implement in practice (Grechka et al., 2006).

Slowness-Polarization Method

In the slowness-polarization method, the slowness vector $\mathbf{p}$ is combined with the polarization vector $\mathbf{U}$ in the inversion for local anisotropy. The slowness method is generally nonlinear

because each source-receiver pair provides one nonlinear eq. (3) for the stiffness coefficients c_{ijkl}. Therefore, application of the slowness method results in a nonlinear inverse problem; the accuracy of the inversion strongly depends on the angular aperture (in terms of the polar and azimuthal angles) of the VSP data (Tsvankin and Grechka, 2011). For TI media, it is essential to acquire data for a wide range of angles with the symmetry axis.

In contrast, inversion of eq. (1) for the stiffnesses using all components of the P-, S_1-, and S_2-wave slowness and polarization vectors is linear (Dewangan and Grechka, 2003). However, including only the polarization vectors and vertical slownesses makes the problem nonlinear.

Still, the addition of the polarization vectors results in a more stable inversion procedure, especially for multicomponent data (de Parscau and Nicoletis, 1990; de Parscau, 1991; Hsu et al., 1991; Horne and Leaney, 2000; Dewangan and Grechka, 2003; Grechka and Mateeva, 2007; Rusmanugroho and McMechan, 2012b,a). Combining the polarization vector with just the vertical slowness makes this method applicable to a subsurface of any complexity, as long as the wavefront at the borehole is close to planar (White et al., 1983; de Parscau, 1991; Hsu et al., 1991; Dewangan and Grechka, 2003; Grechka et al., 2007).

Dewangan and Grechka (2003) invert the vertical slownesses and polarization vectors of P-, S_1- and S_2-waves for the full stiffness tensor of a triclinic medium without a priori symmetry assumptions. They show, however, that the inversion becomes unstable and produces significant errors, if the horizontal slowness components cannot be estimated because of lateral heterogeneity.

Application of Slowness-Polarization Inversion to VTI Media

According to de Parscau (1991) and Hsu et al. (1991), joint inversion of the vertical slowness components and polarization vectors of P- and SV-waves in VTI media can constrain the P- and S-wave vertical velocities (V_{P0} and V_{S0}) and anisotropy coefficients δ and ϵ. Grechka and Mateeva (2007) apply this approach to P-wave only and identify the following modified anisotropy coefficients constrained by the P-wave vertical slowness and polarization angle:

$$\delta_{VSP} = (f_0 - 1)\delta\,, \tag{5}$$

$$\eta_{VSP} = (2f_0 - 1)\eta\,, \tag{6}$$

$$f_0 = \frac{1}{1 - V_{S0}^2/V_{P0}^2}. \tag{7}$$

Here η is the anellipticity parameter introduced by Alkhalifah and Tsvankin (1995):

$$\eta = \frac{\epsilon - \delta}{1 + 2\delta}\,. \tag{8}$$

The polarization vector $\mathbf{U}$ in VTI media is typically defined by the angle ψ that it makes with the vertical symmetry axis. By applying perturbation theory (Backus, 1965; Pšenčík and Gajewski, 1998; Farra, 2001) in the weak-anisotropy approximation (WAA), the P-wave vertical slowness component $p_{3,p} = q_P(\psi)$ can be found as the following function of the angle ψ (Grechka and Mateeva, 2007):

$$q_P(\psi) \approx \frac{\cos\psi}{V_{P0}}\left[1 + \delta_{VSP}\,\sin^2\psi + \eta_{VSP}\,\sin^4\psi\right]. \tag{9}$$

Whereas δ_{VSP} controls eq. (9) for near-offset data (small angles ψ), the contribution of η_{VSP} increases with angle. Equation 9 shows that both effective parameters, δ_{VSP} and η_{VSP}, can be constrained by P-wave data provided the survey aperture is sufficiently wide. To convert δ_{VSP} and η_{VSP} into δ and η, it is necessary to obtain V_{S0} from S-wave data [eqs. (5)-(7)]. SV-waves, however, may also provide useful additional constraints on the anisotropy parameters, as discussed below.

APPROXIMATE SLOWNESS-POLARIZATION RELATIONSHIP FOR SV-WAVES

To gain insight into the parameters that control the relationship between the vertical slowness and polarization angle for SV-waves, we derived the following weak-anisotropy approximations (Appendix A):

$$q_{SV}(\psi_{SV}) = \frac{\sin\psi_{SV}}{V_{S0}}[1 + (f_0\delta - \sigma)\cos^2\psi_{SV} + (\sigma + 2f_0\eta)\cos^4\psi_{SV}] \tag{10}$$

$$= \frac{\sin\psi_{SV}}{V_{S0}}[1 + f_0(\epsilon - \sigma)\cos^2\psi_{SV} + f_0(\sigma + \eta)\cos^4\psi_{SV}]\,, \tag{11}$$

where ψ_{SV} is the angle between the SV-wave polarization vector and the vertical and σ is a parameter that largely controls SV-wave anisotropy (Tsvankin, 2012):

$$\sigma = \left(\frac{V_{P0}}{V_{S0}}\right)^2(\epsilon - \delta) \approx \left(\frac{V_{P0}}{V_{S0}}\right)^2\eta. \tag{12}$$

Fig. 1 shows that the approximations from eqs. (9) and (11) are close to the exact solutions for P- and SV-waves in typical moderately anisotropic VTI models.

According to eqs. (10) and (11), the function $q_{SV}(\psi_{SV})$ is controlled by the anisotropy

coefficients η and ϵ or η and δ (σ is a simple function of η, see eq. 12). Note that at polarization angles around 45°, the function q_{SV} is mostly dependent on the parameter δ. Therefore, the weak-anisotropy approximation for $q_{SV}(\psi_{SV})$ indicates that wide-aperture SV data provide valuable information for estimating both η and δ.

The condition numbers for both P- and SV-waves computed from eqs. (9) and (10) with different V_{P0}/V_{S0} ratios are shown in Fig. 2. A large condition number indicates that a small error in the data can cause a significant distortion in the estimated parameters. Clearly, SV-waves provide tighter constrains on the anisotropy parameters than P-waves, especially for larger V_{P0}/V_{S0} ratios.

To calculate the exact vertical slowness components of P- and SV-waves from the polarization angle ψ, Grechka and Mateeva (2007) derived the following quadratic equation:

$$(c_{11} - c_{55}) \tan^2\theta + 2(c_{13} + c_{55}) \cot 2\psi \tan\theta - (c_{33} - c_{55}) = 0\,, \tag{13}$$

where θ is the phase angle with the symmetry axis. Except for uncommon VTI models, the two roots of eq. (13) yield the phase angles of the P- and SV-waves, whose polarization directions are specified by angle ψ. The phase angle for P-waves corresponds to the solution with a smaller value of $|\theta - \psi|$. The exact phase velocity and vertical slownesses q_P and q_{SV} can then be obtained by substituting the angles θ_P and θ_S into the Christoffel equation. In the inversion, the best-fit values of δ and η can be found using the available pairs of the parameters ψ and q.

The exact and approximate functions $q(\psi)$ for a range of δ ($0 \le \delta \le 0.30$) and η ($0 \le \eta \le 0.30$) values are displayed in Fig. 3. The P-wave signature is weakly dependent on both δ and η when the coefficients vary within the chosen range. Therefore, a small measurement

error in the P-wave vertical slowness or polarization angle can cause a significant distortion in the estimated anisotropy parameters. In contrast, the SV-wave function $q(\psi_{SV})$ is much more sensitive to δ and η, as predicted by the condition number in Fig. 2.

INVERSION METHODOLOGY

Extending the approach by Grechka and Mateeva (2007), we use the vertical slowness components and the corresponding polarization angles of P- and SV-waves to estimate the local VTI parameters. The model and data vectors are given by:

$$\mathbf{m} = \{\delta,\, \eta\}, \tag{14}$$

$$\mathbf{d} = \{q_P(\psi_P),\, q_{SV}(\psi_{SV})\}. \tag{15}$$

where $\mathbf{d}$ contains all available pairs of q and ψ for a given receiver. The interval vertical velocities V_{P0} and V_{S0} can be calculated from VSP data generated by sources near the well head. When such "zero-offset" sources are not available or produce low-quality data, both velocities can be estimated along with δ and η. This, however, makes the inversion process more time consuming and less stable.

To determine the direct-arrival traveltimes, we pick the first breaks of P- and SV-waves from the records of vertical and horizontal sources, respectively. The quality of first-break picking directly impacts the accuracy of the measured polarization angles and vertical slownesses. To prevent abrupt changes in the values of q and reduce estimation errors, the vertical slownesses are computed from the traveltimes for three adjacent geophones.

As emphasized by Grechka and Mateeva (2007), the linearity of the particle motion is essential for ensuring a high quality of polarization estimates. Therefore, data with a noticeably nonlinear particle motion should be removed. Similar to the vertical slowness, the polarization angles are obtained as the average of measurements for three adjacent geophones.

The model vector $\mathbf{m}$ is estimated by minimizing the following objective function:

$$E(\mathbf{m}) = W_P \, \Sigma[q_P^{\text{calc}}(\mathbf{m}, \psi_P) - q_P(\psi_P)]^2 + W_{SV} \, \Sigma[q_{SV}^{\text{calc}}(\mathbf{m}, \psi_{SV}) - q_{SV}(\psi_{SV})]^2, \qquad (16)$$

where W_P and W_{SV} are the weights of the P- and SV-wave contributions, which can be adjusted based on the desired scenario, data quality, and errors in q and ψ. When only P-wave data are used, $W_P = 1.0$ and $W_{SV} = 0.0$; for joint inversion without a priori model information, we set $W_P = 0.5$ and $W_{SV} = 0.5$. The sum in eq. (16) includes all data points for a given receiver. The modeled functions q_P and q_{SV} are computed exactly using eq. (13) and then the Christoffel equation, with the weak-anisotropy approximations (9) and (11) employed to find the initial parameter values.

SYNTHETIC EXAMPLE

Data Processing

The proposed technique was tested on the four-layer model in Fig. 4. The multicomponent data were computed for 61 source locations using both vertical and horizontal sources (point forces) with a finite-difference algorithm (Fig. 5). To enhance the quality of first-break picking, especially for far-offset shots, the geophone records for both vertical and horizontal

sources were rotated to maximize the P- or SV-wave energy on one of the components.

As mentioned above, stable calculation of the polarization angle requires that the particle motion be close to linear. The linearity of the particle motion for P-, pure SV- and converted SV-waves is evaluated in Fig. 6. To reduce the nonlinearity of particle motion, we recommend using a short time window for hodogram analysis (e.g., one-half of the cycle of the first arrival). This approach increases the accuracy of polarization measurements in the presence of strong multiples or upgoing waves. It is also helpful to smooth the polarization data using a 2D moving averaging window (based on the source offset and receiver depth).

The interval vertical velocities V_{P0} and V_{S0} were calculated using the first-break arrivals from the source located 100 m away from the well. The errors in both velocities do not exceed 2%.

Parameter Estimation

The inversion for δ and η was carried out using three different approaches, one of which operates just with P-waves and the other two combine P-wave data with either pure SV-waves or mode-converted PSV data. As an example, Fig. 7 depicts the best-fit $q(\psi)$ functions (dashed lines) and measured P- and pure SV-wave data for a group of three receivers, centered at 2000 m depth. Also, it shows the errors in the data for models with different pairs of δ and η. The addition of SV-waves to P-wave data yields more accurate anisotropy parameters (Figs. 7c,d) and helps improve the fit for the SV-wave slowness-polarization function (Figs. 7a,b).

Comparing the estimated parameters δ and η with the actual values for the entire receiver array (Fig. 8) demonstrates the advantages of using both P- and SV-wave data.

The joint inversion of P- and SV-waves produces a more close match to the actual $\delta-$ and $\eta-$functions than that for the P-wave algorithm. Even the joint method, however, cannot estimate the anisotropy parameters with sufficient accuracy near the medium interfaces.

The parameters δ and η were also estimated using different P-wave (W_P) and SV-wave (W_{SV}) weight combinations (Fig. 9 and 10). The sensitivity analysis confirms the advantage of involving both P- and SV-wave data in the inversion process, with the smallest error corresponding to similar values of the weights W_P and W_{SV}. Note that Fig. 10 analyzes the accuracy of the algorithm for specific model parameters and acquisition geometry. Therefore, the optimal combination of W_P and W_{SV} from Fig. 10 will not necessarily work for other cases. As mentioned before, assigning the same weight to P and SV data when we do not have sufficient information about the model should be the best strategy. However, if we have rough estimates of the anisotropy parameters in the receiver layer, W_P and W_{SV} can be adjusted accordingly.

Regardless of the input data for the inversion, the slowness-polarization method produces significant errors at the layer boundaries. These distortions are caused by the difference in the properties of the overlying and underlying layers in the analysis window and the presence of reflections (upgoing waves), which distort the estimated polarization angle.

Because acquiring pure S-waves (generated by horizontal sources) is not common, and many VSP surveys record converted PS data using 3C geophones, the joint inversion approach was also applied with P- and PSV-waves. The results of the joint inversion of P- and PSV-wave data in Fig. 11 are inferior to those obtained with P- and pure SV-waves. In terms of input data, there is no difference between pure SV and PSV in the inversion, because the vertical slowness and polarization vectors are local properties near the receiver.

The better performance of pure SV-waves in the inversion is explained primarily by their larger aperture compared to mode conversions (Fig. 12). For the model in Fig. 4, the range of polarization angles for PSV-waves is, on average, 30° smaller than that for pure SV-waves. It may be possible to somewhat increase the aperture by using reflected PSV-waves. However, even PSV reflections have a limited range of propagation angles with the vertical due to Snell's law. Also, we seldom have good-quality shear-wave reflections and estimating polarization angles for direct waves is easier than for reflected waves (which often interfere with other modes).

Also, pure SV-wave data have a more linear particle motion compared to PSV-waves (see Fig. 6), which helps determine the SV-wave polarization angle with higher accuracy. The nonlinear particle motion of PSV-waves is mostly due to their interference with P-wave multiples and reflections. Certain processing steps (like wavefield separation) might produce more accurate measurements of SV-wave polarization.

CONCLUSIONS

We generalized the P-wave slowness-polarization methodology for VTI media proposed by Grechka and Mateeva for the combination of P and SV data. The derived analytic approximation for the relationship between the SV-wave vertical slowness and polarization angle shows that SV data provide valuable information for estimating both δ and η. The inversion results strongly depend on the data quality (especially that for shear waves), angle coverage, and the size of the depth window in the analysis (which may be based on local stratigraphy).

Synthetic testing for a layered VTI model confirmed the advantages of the joint P-

and SV-wave slowness-polarization method compared to the inversion operating with just P-waves. Also, because of their larger aperture and more linear particle motion, pure SV-waves perform better in the slowness-polarization method compared to converted PSV data. One of the remaining challenges is accurate parameter estimation near layer boundaries.

ACKNOWLEDGMENTS

This research was conducted at the Reservoir Characterization Project (RCP) at Colorado School of Mines. We also acknowledge the support of the Center for Wave Phenomena (CWP) at CSM. We thank Mike O'Brien (Allied Geophysics Inc.) for generating synthetic VSP data for this research and Vladimir Grechka (Marathon Oil Corp.) for his scientific and technical advice. We also would like to acknowledge Rich Van Dok and Brian Fuller (Sigma Cubed Inc.) for providing software and support for this work. The thorough review of the journal referee helped improve the paper.

APPENDIX A

WEAK-ANISOTROPY APPROXIMATION FOR THE SV-WAVE VERTICAL SLOWNESS IN VTI MEDIA

Here, we obtain the relationship between the SV-wave vertical slowness and polarization angle for VTI media in the weak-anisotropy approximation. The angle between the P-wave polarization vector and the symmetry axis can be found from the following expression linearized in the anisotropy parameters (Tsvankin, 2012, eq. (1.78)):

$$\psi_P = \theta + \psi^{AN}\,, \tag{A-1}$$

where θ is the phase angle with the symmetry axis and ψ^{AN} is the anisotropic term:

$$\psi^{AN} = f_0(\delta + 2\eta \sin^2\theta) \sin\theta \cos\theta = \frac{1}{2} f_0 \sin 2\theta (\delta + 2\eta \sin^2\theta)\,; \tag{A-2}$$

$$f_0 = \left(1 - \frac{{V_{S0}}^2}{{V_{P0}}^2}\right)^{-1}. \tag{A-3}$$

Suppose ν_{SV} is the angle between the SV-wave polarization vector and the horizontal (Fig. 13). Then, taking into account that the P- and SV-wave polarization vectors for the same phase direction are orthogonal, we can find ν_{SV} as

$$\nu_{SV} = \psi_P = \theta + \psi^{AN}, \tag{A-4}$$

The SV-wave velocity in the weak-anisotropy approximation has the form:

$$V_{SV}(\theta) = V_{S0}\,(1 + \sigma \sin^2\theta \cos^2\theta). \tag{A-5}$$

Hence, the SV-wave slowness linearized in the anisotropy parameters is given by

$$p_{SV}(\theta) = \frac{1}{V_{SV}(\theta)} \approx \frac{1}{V_{S0}}\,(1 - \sigma \sin^2\theta \cos^2\theta)\,, \tag{A-6}$$

and the vertical slowness component of the SV-wave is (note that in the anisotropic terms θ and ν_{SV} are interchangeable):

$$p_{3,SV}(\theta) = q_{SV}(\theta) = \frac{\cos\theta}{V_{S0}}(1 - \sigma \sin^2\theta \cos^2\theta) \approx \frac{\cos\theta}{V_{S0}}(1 - \sigma \sin^2\nu_{SV} \cos^2\nu_{SV}). \tag{A-7}$$

Substituting the phase angle from eq. (A-4) into eq. (A-7) yields:

$$q_{SV} = \cos(\nu_{SV} - \psi^{AN})\,\frac{1 - \sigma \sin^2 \nu_{SV} \cos^2 \nu_{SV}}{V_{S0}}. \tag{A-8}$$

The term $\cos(\nu_{SV} - \psi^{AN})$ can be rewritten as:

$$\cos(\nu_{SV} - \psi^{AN}) = \cos \nu_{SV} \cos \psi^{AN} + \sin \nu_{SV} \sin \psi^{AN} \approx \cos \nu_{SV} + \psi^{AN} \sin \nu_{SV}. \tag{A-9}$$

Substituting eq. (A-9) into eq. (A-8) and keeping terms linear in the anisotropy coefficients, we find:

$$q_{SV}(\nu_{SV}) = \frac{\cos \nu_{SV}}{V_{S0}}\,[1 - \sigma \sin^2 \nu_{SV} \cos^2 \nu_{SV} + \psi^{AN} \tan \nu_{SV}]. \tag{A-10}$$

Using eq. (A-2), the term $\psi^{AN} \tan \nu_{SV}$ can be expressed through ν_{SV} (again, here θ can be replaced with ν_{SV} in the weak-anisotropy approximation):

$$\begin{aligned} \psi^{AN} \tan \nu_{SV} &= \frac{1}{2} \tan \nu_{SV}\, f_0 \sin 2\theta (\delta + 2\eta \sin^2 \theta) \\ &\approx f_0 \sin^2 \nu_{SV} (\delta + 2\eta \sin^2 \nu_{SV}). \end{aligned} \tag{A-11}$$

Substitution of eq. (A-11) into eq. (A-10) leads to:

$$q_{SV}(\nu_{SV}) = \frac{\cos \nu_{SV}}{V_{S0}}\,[1 + (f_0\,\delta - \sigma) \sin^2 \nu_{SV} + (\sigma + 2 f_0 \eta) \sin^4 \nu_{SV}]. \tag{A-12}$$

Eq. (A-12) can be represented in terms of the SV-wave polarization angle with the vertical ($\psi_{SV} = \pi/2 - \nu_{SV}$):

$$q_{SV}(\psi_{SV}) = \frac{\sin\psi_{SV}}{V_{S0}}\,[1 + (f_0\,\delta - \sigma)\cos^2\psi_{SV} + (\sigma + 2f_0\eta)\cos^4\psi_{SV}]. \tag{A-13}$$

Next, we separate f_0 in the anisotropic terms in eq. (A-13):

$$\begin{aligned} f_0\delta - \sigma &= f_0(\epsilon - \sigma)\,, \\ \delta + 2f_0\eta &= f_0(\sigma + \eta). \end{aligned} \tag{A-14}$$

Finally, eqs. A-14 allow us to rewrite eq. (A-13) as:

$$q_{SV}(\psi_{SV}) = \frac{\sin\psi_{SV}}{V_{S0}}\,[1 + f_0(\epsilon - \sigma)\cos^2\psi_{SV} + f_0(\sigma + \eta)\cos^4\psi_{SV}]. \tag{A-15}$$

REFERENCES

Alkhalifah, T. and Tsvankin, I., 1995. Velocity analysis for transversely isotropic media. Geophysics, 60: 1550-1566.

Backus, G. E., 1965. Possible form of seismic anisotropy of the upper most mantle under ocean. Journal of Geophysical Research, 70: 3429-3439.

de Parscau, J., 1991. Relationship between phase velocities and polarization in transversely isotopic media. Geophysics, 56: 1578-1583.

de Parscau, J., and Nicoletis, L., 1990. Tranverse isotropy estimation from multioffset VSPs. 60th SEG Annual Meeting, SEG Technical Program Expanded Abstract, 1439-1442.

Dewangan, P., and Grechka, V., 2003. Inversion of multicomponent, multiazimuthal, walk-away VSP data for stiffness tensor. Geophysics, 68: 1022-1031.

Farra, V., 2001. Higher-order perturbation of the phase velocity and polarization of qP and qS waves in anisotropic media. Geophysical Journal International, 147: 93-104.

Gaiser, J. E., 1990. Transversely isotropic phase velocity analysis from slowness estimates. Journal of Geophysical Research, 95: 11241-11254.

Grechka, V., Jorgensen, P. , and Lopez, J. L., 2006. Anisotropy estimation from marine 3D VSP data. Offshore Technology Conference, OTC17866.

Grechka, V., and Mateeva, A., 2007. Inversion of P-wave VSP data for local anisotropy: Theory and case study. Geophysics, 72: D69-79.

Grechka, V., Mateeva, A., Gentry, C., Jorgensen, P., and Lopez, J. L., 2007. Estimation of seismic anisotropy from P-wave VSP data. The Leading Edge, 26: 756-759.

Horne, S., and Leaney, S., 2000. Short note: Polarization and slowness component inversion for TI anisotropy. Geophysical Prospecting, 48: 779-788.

Hsu, K., Schoenberg, M., and Walsh, J., 1991. Anisotropy from polarization and moveout: A case study. 61st SEG Annual Meeting, SEG Technical Program Expanded Abstract, 1526-1529.

Jílek, P., Hornby, B., and Ray, A., 2003. Inversion of 3D VSP P-wave data for local anisotropy: A case study. 73rd SEG Annual Meeting, SEG Technical Program Expanded Abstract, 1322-1325.

Miller, D. E., and Spencer, C., 1994. An exact inversion for anisotropic moduli from phase slowness data. Journal of Geophysical Research, 99: 21651-21657.

Pevzner, R., Guervich, B., and Urosevic, M., 2011. Estimation of azimuthal anisotropy from VSP data using multicomponent S-wave velocity analysis. Geophysics, 76: D1-D9.

Pšenčík, I., and Gajewski, D., 1998. Polarization, phase velocity, and NMO velocity of qP-waves in arbitrary weakly anisotropic media. Geophysics, 63: 1754-1766.

Rusmanugroho, H., and McMechan, G. A., 2012a. 3D 9C seismic modeling and inversion of Weyburn field data. Geophysics, 77: R161-R173.

Rusmanugroho, H., and McMechan, G. A., 2012b. Sensitivity of estimated elastic moduli to completeness of wave type, measurement type, and illumination aperture at a receiver in multicomponent VSP data. Geophysics, 77: R1-R18.

Tsvankin, I., 2012. Seismic signature and analysis of reflection data in anisotropic media, third edition. Society of Exploration Geophysicists.

Tsvankin, I., and Grechka, V., 2011. Seismology of azimuthally anisotropic media and seismic fracture characterization. Society of Exploration Geophysicists.

White, J. E., Martineau-Nicoletis, L., and Monash, C., 1983. Measured anisotropy in Pierre shale. Geophysical Prospecting, 31: 709-725.

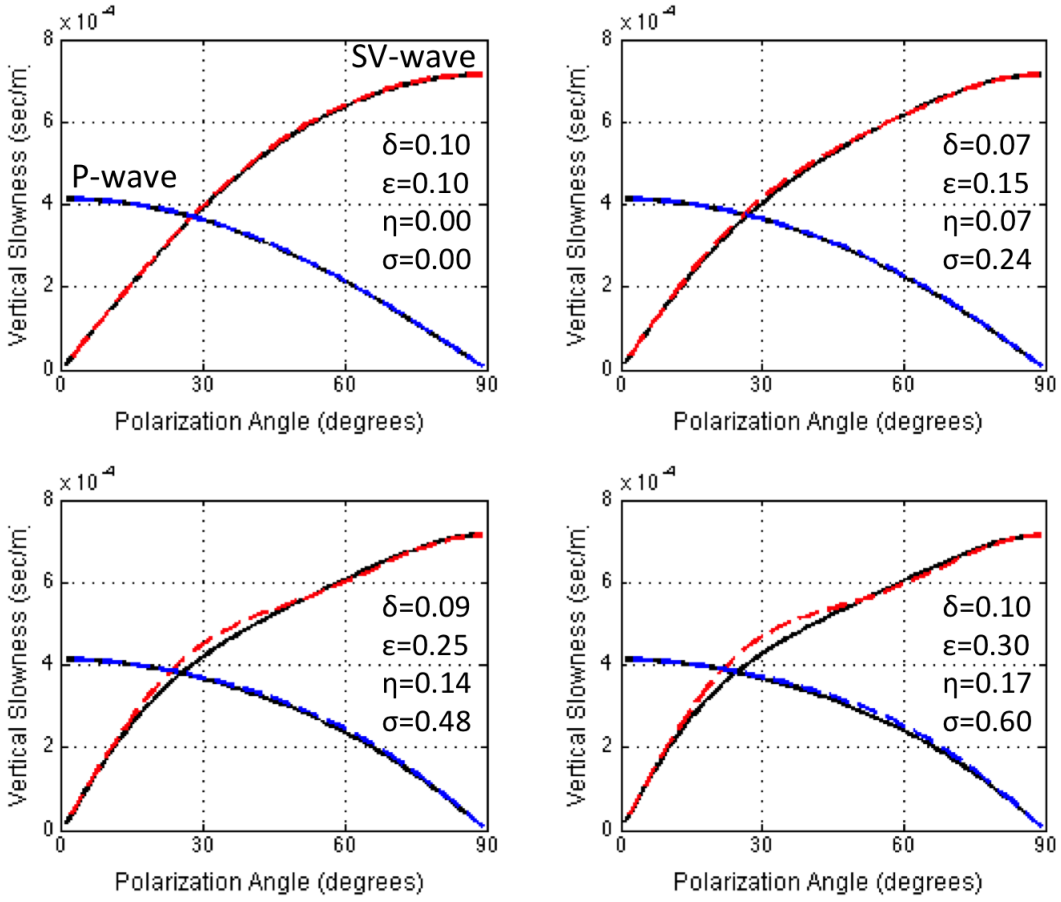

Fig. 1: Exact vertical slowness (q) as a function of the polarization angle (ψ) for P- and SV-waves (solid curves) and the corresponding weak-anisotropy approximations computed from eqs. (9) and (11) (dashed curves). The plots correspond to four VTI models with V_{P0}=2420 m/s and V_{S0}=1400 m/s (the models are taken from Tsvankin, 2012).

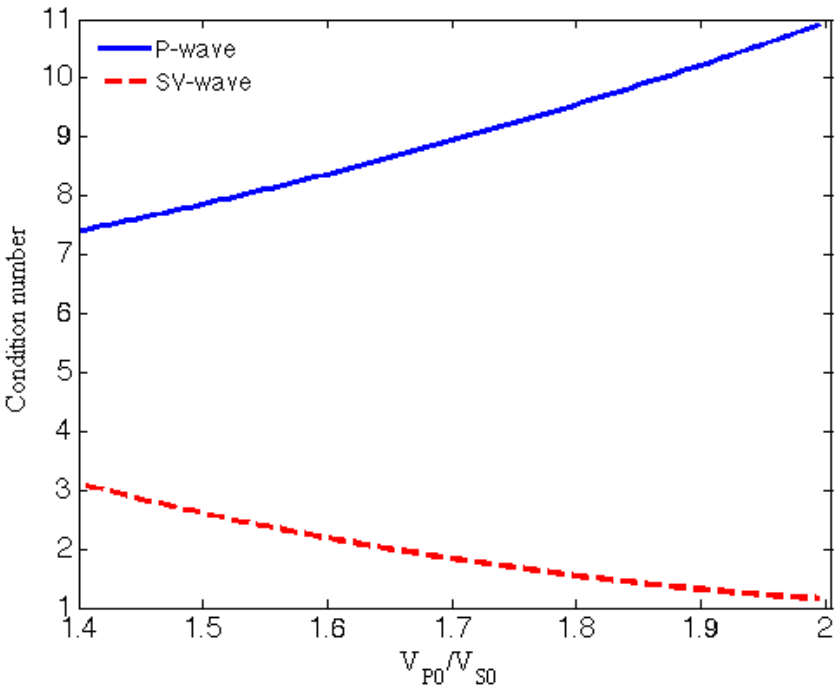

Fig. 2: Condition number calculated as a function of the V_{P0}/V_{S0} ratio for P-waves from eq. (9) and SV-waves from eq. (10).

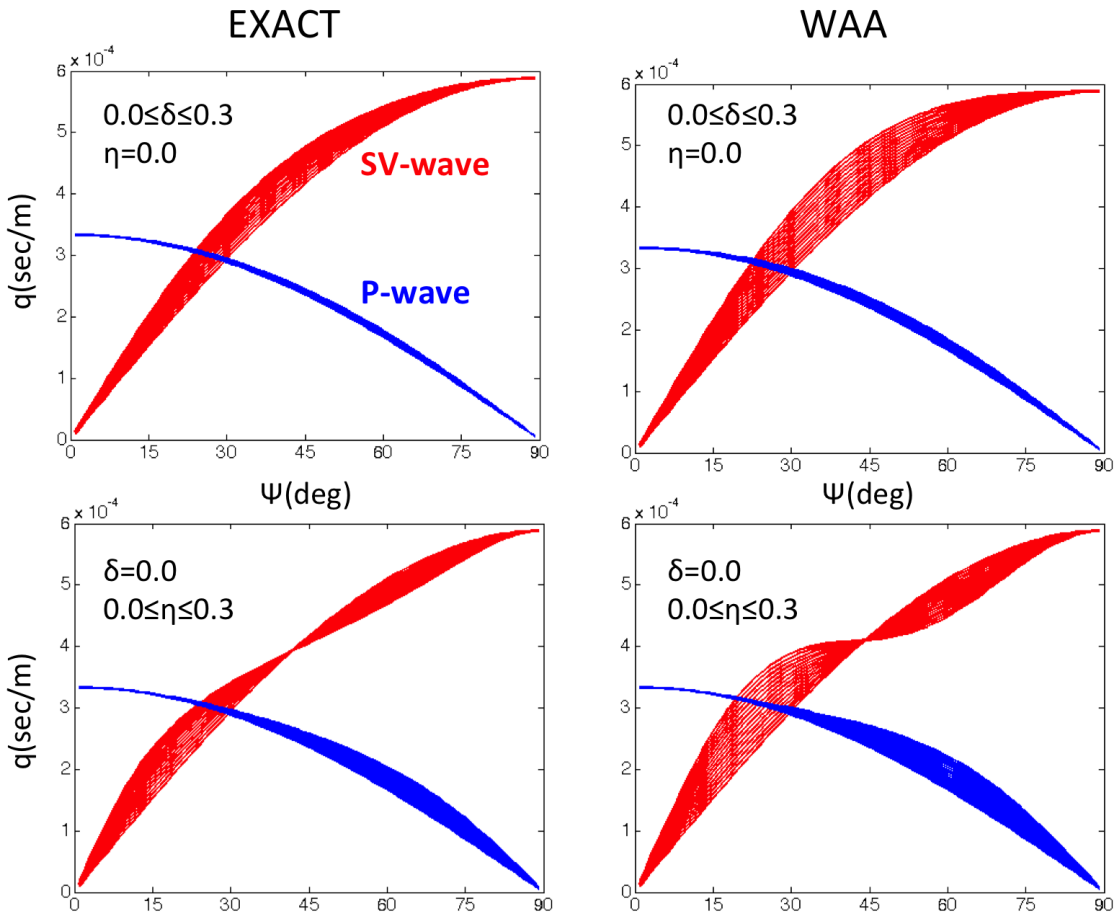

Fig. 3: Relationship between the vertical slownesses and polarization angles of P- and SV-waves for a range of δ- and η-values ($V_{P0}/V_{S0} = 1.76$). The curves on the left plots are computed from the exact equations and on the right plots from the weak-anisotropy approximations.

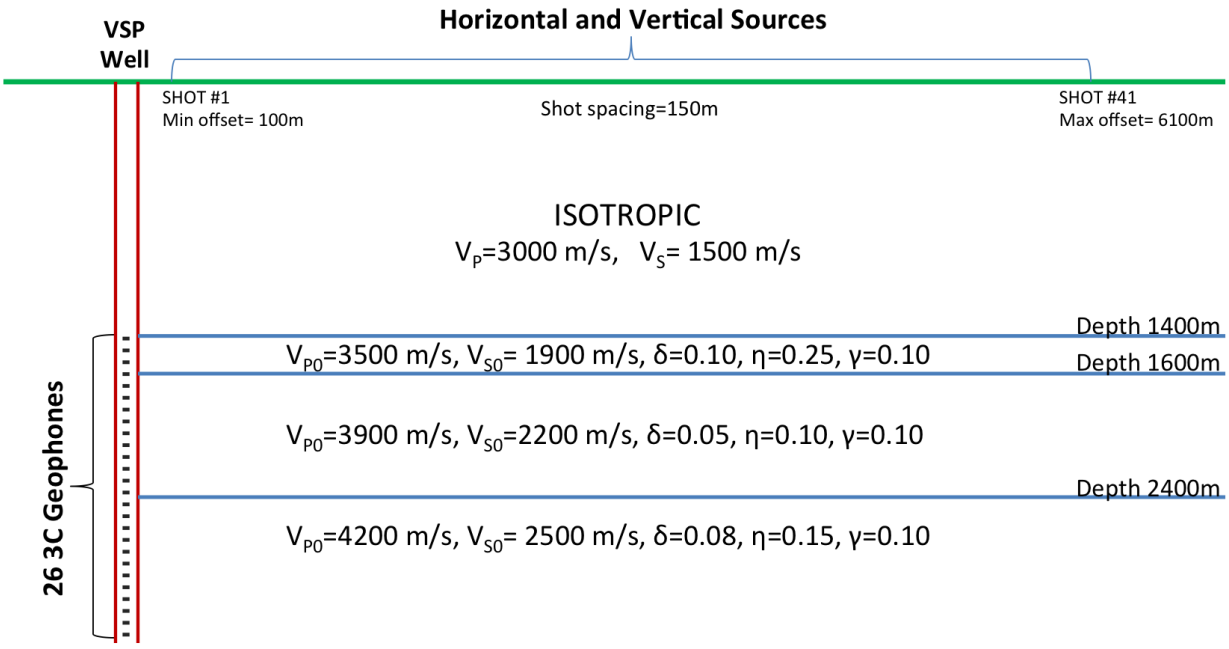

Fig. 4: Model used to generate 9C VSP data. The three bottom layers are VTI and the near-surface layer is isotropic. The density for all layers is equal to 2.28 g/cc. Horizontal and vertical sources (point forces) are deployed every 150 m at distances from 100 m to 6100 m away from the well. The data are recorded by 26 geophones placed in the borehole between 1400 m and 2900 m with a 60 m spacing.

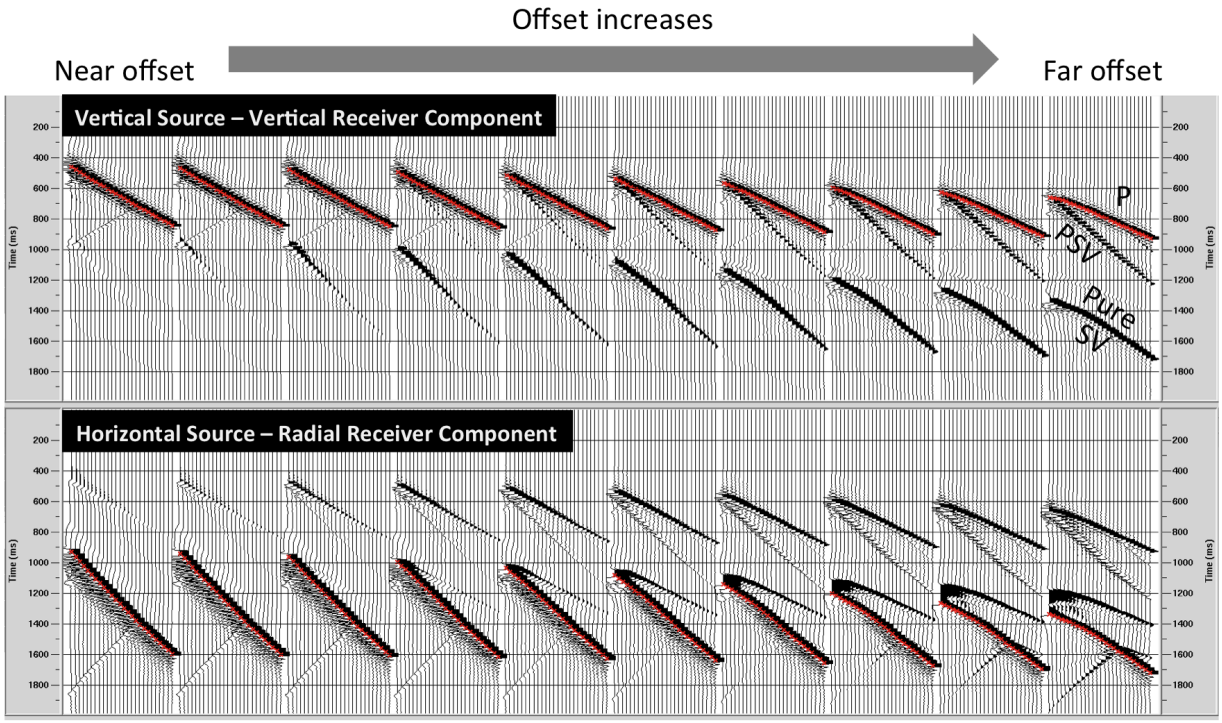

Fig. 5: Ten examples (out of 61) of the recorded vertical displacement component from a vertical source (top) and the radial component from a horizontal source (bottom). The source offset increases from left to right. See the caption of Fig. 4 for the recording geometry.

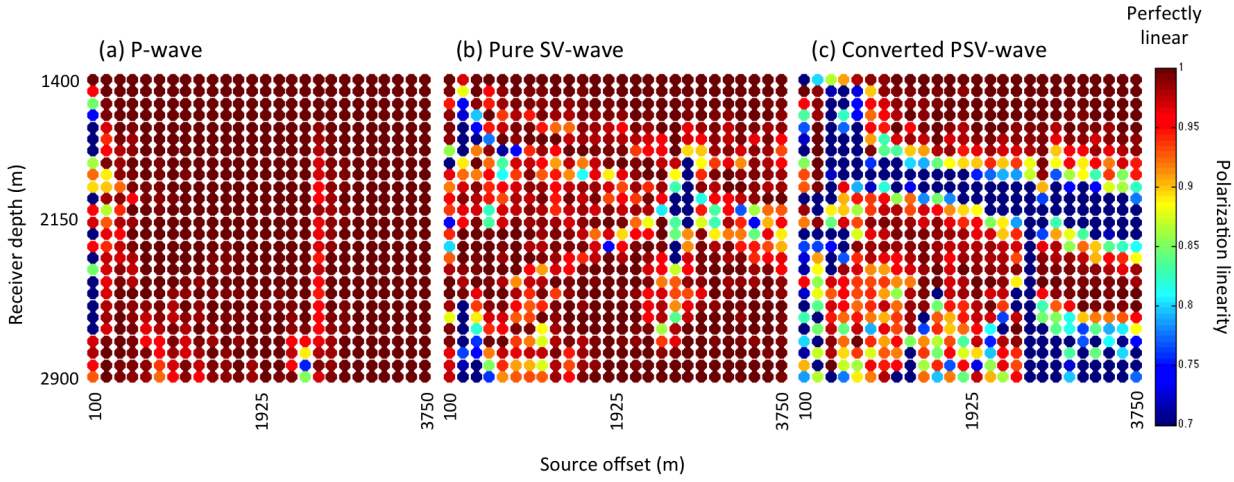

Fig. 6: Linearity of the particle motion for P-waves, pure SV-waves and converted PSV-waves. Unity corresponds to a linear particle motion, while zero means that the particle motion is circular.

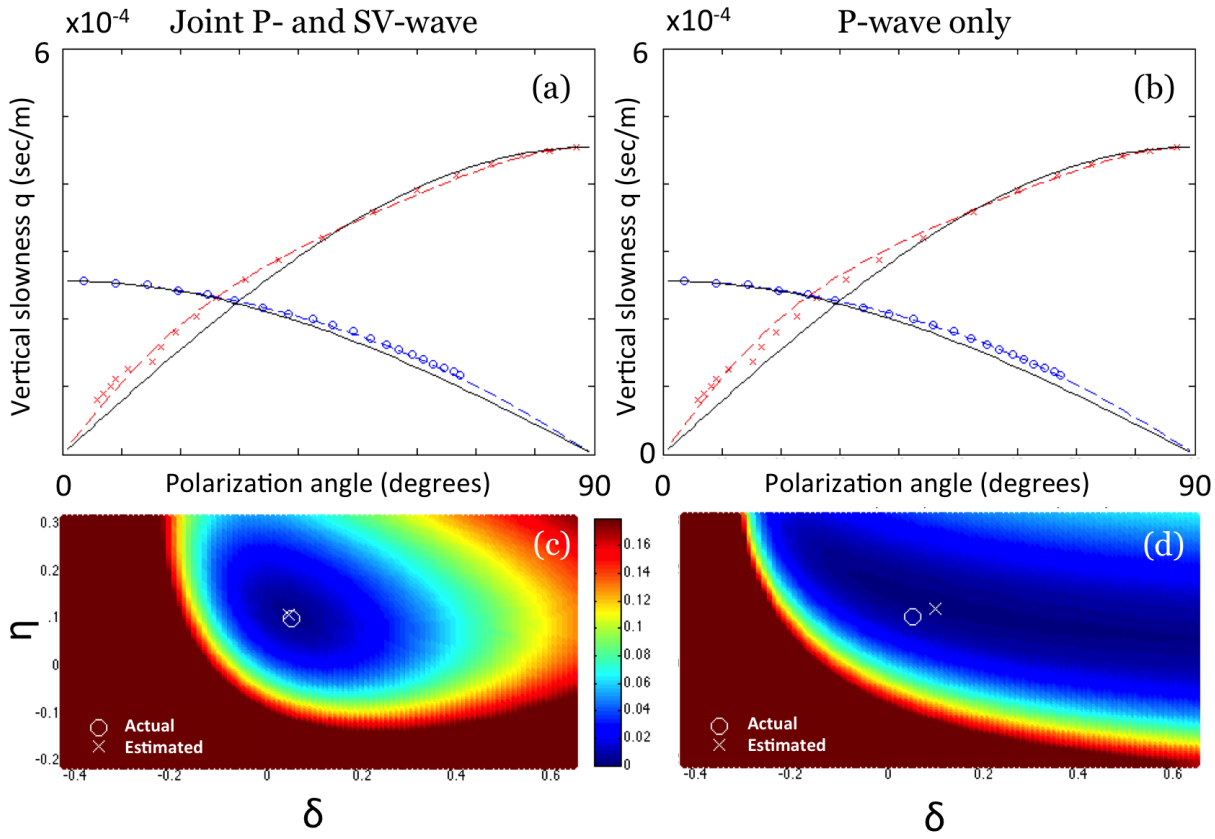

Fig. 7: Results obtained using the joint inversion of P- and SV-waves (a, c) and P-waves only (b, d). Plots (a, b) show the inversion results for receiver group no. 10, which includes three receivers centered at a depth of 2000 m. The dashed lines mark the best-fit $q(\psi)$ functions, and the data are marked by circles (P-waves) and crosses (SV-waves). The weighted SSE (sum of squared errors) maps on plots (c) and (d) show the difference between the data modeled with different δ and η pairs and picked from the synthetic seismograms. The actual parameters are marked by circles, and estimated parameters by crosses.

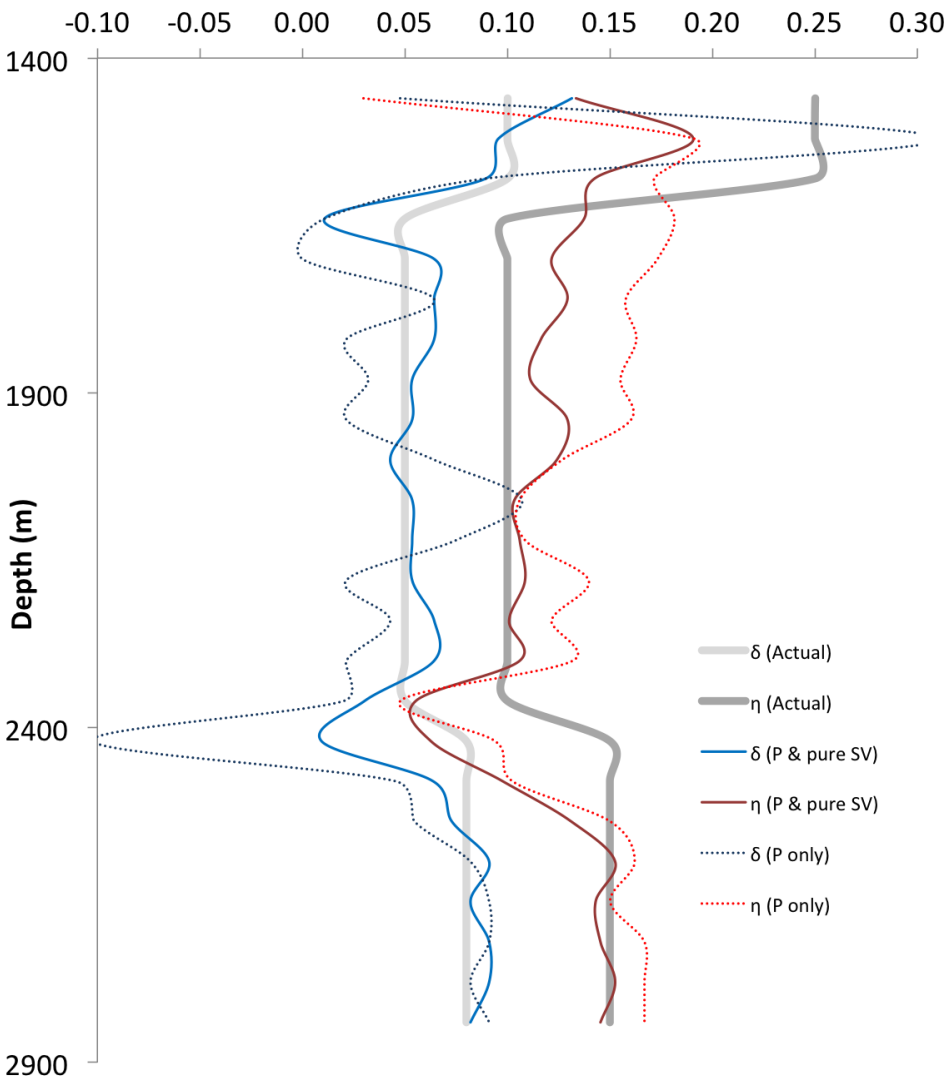

Fig. 8: Estimated parameters δ and η along the well. The results of inverting solely P-waves are marked by dotted lines and of the joint inversion of P and pure SV data by solid lines. The actual δ- and η-values (using a 3-geophone averaging window) are marked by light thick lines.

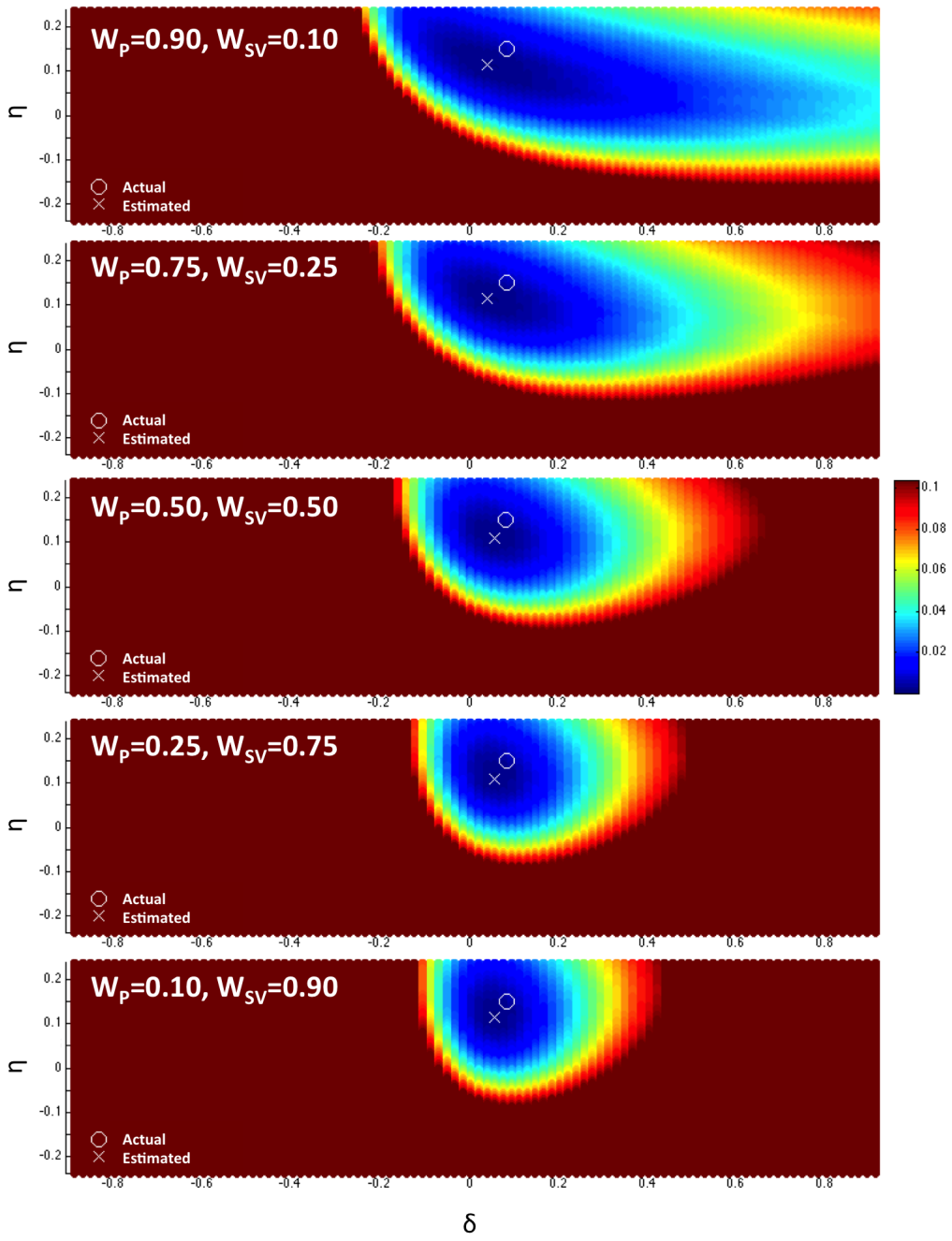

Fig. 9: Sensitivity of the inversion results to the weights W_P and W_{SV} shown on the maps. Each map displays the difference between the data ($q(\psi)$ functions for P- and SV-waves) for receiver no. 18 and model data computed for different pairs of δ and η. The minimum error on each map corresponds to the estimated parameters and is marked with a cross. The actual parameters are marked with circles.

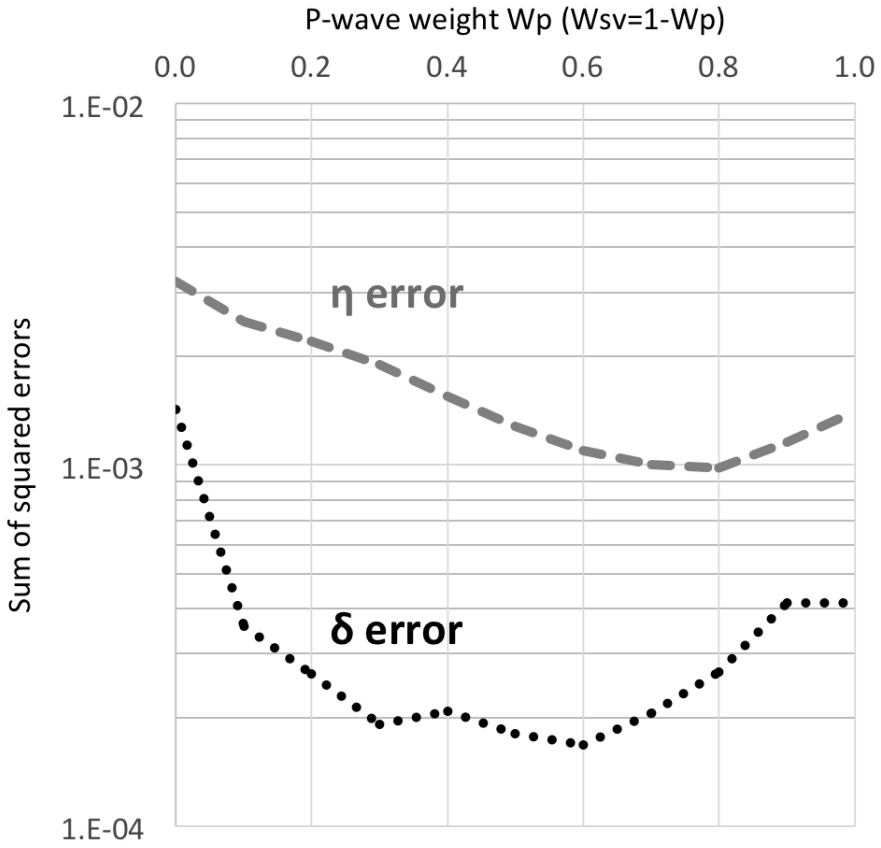

Fig. 10: Summary of estimation errors in δ and η for different W_P and W_{SV} combinations and the entire VSP interval.

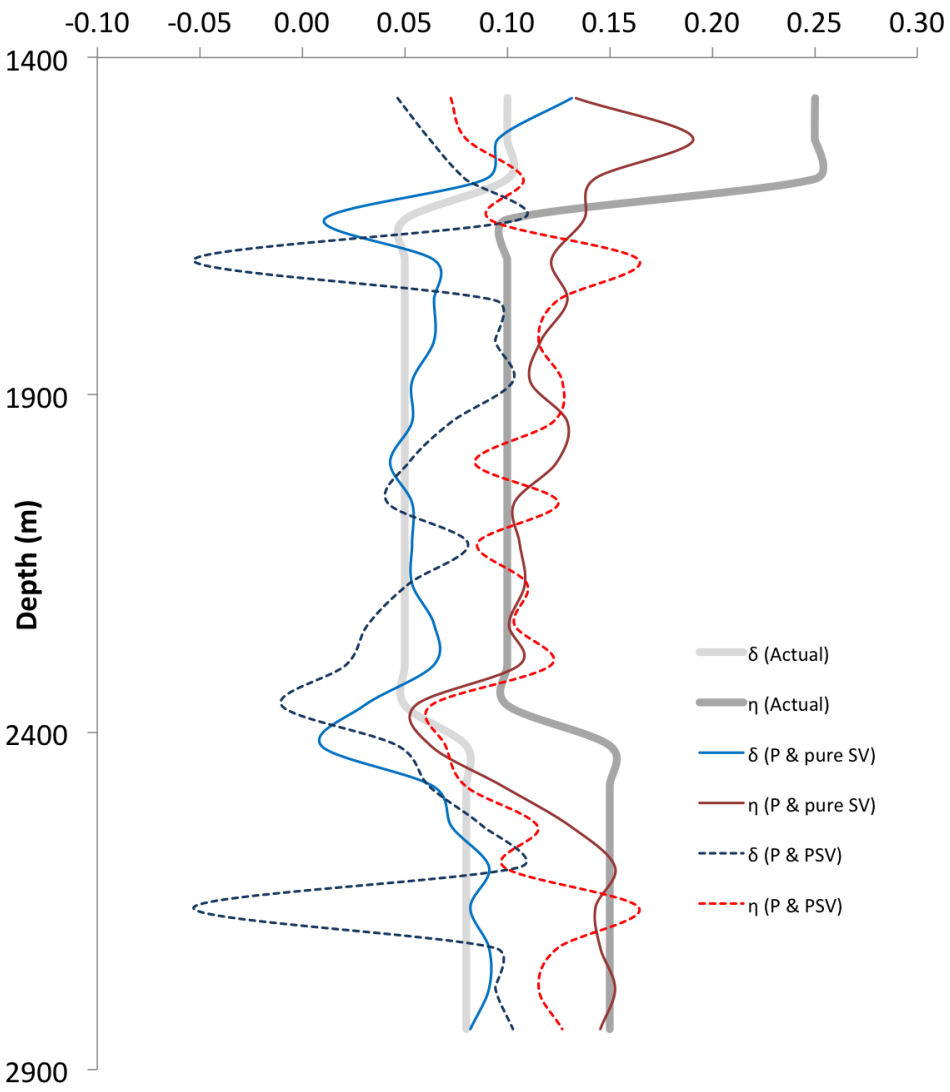

Fig. 11: Parameters δ and η estimated using P- and converted PSV-wave data (dotted lines) and P- and pure SV-waves (solid lines). The actual δ and η values (using a 3-geophone averaging window) are marked by light thick lines.

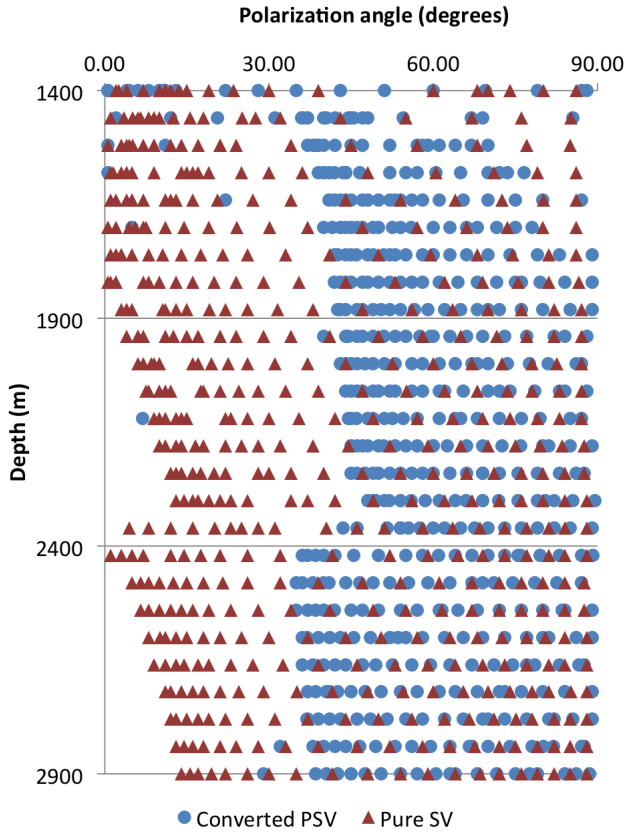

Fig. 12: Polarization angles of pure SV- and converted PSV-waves used in the joint inversion.

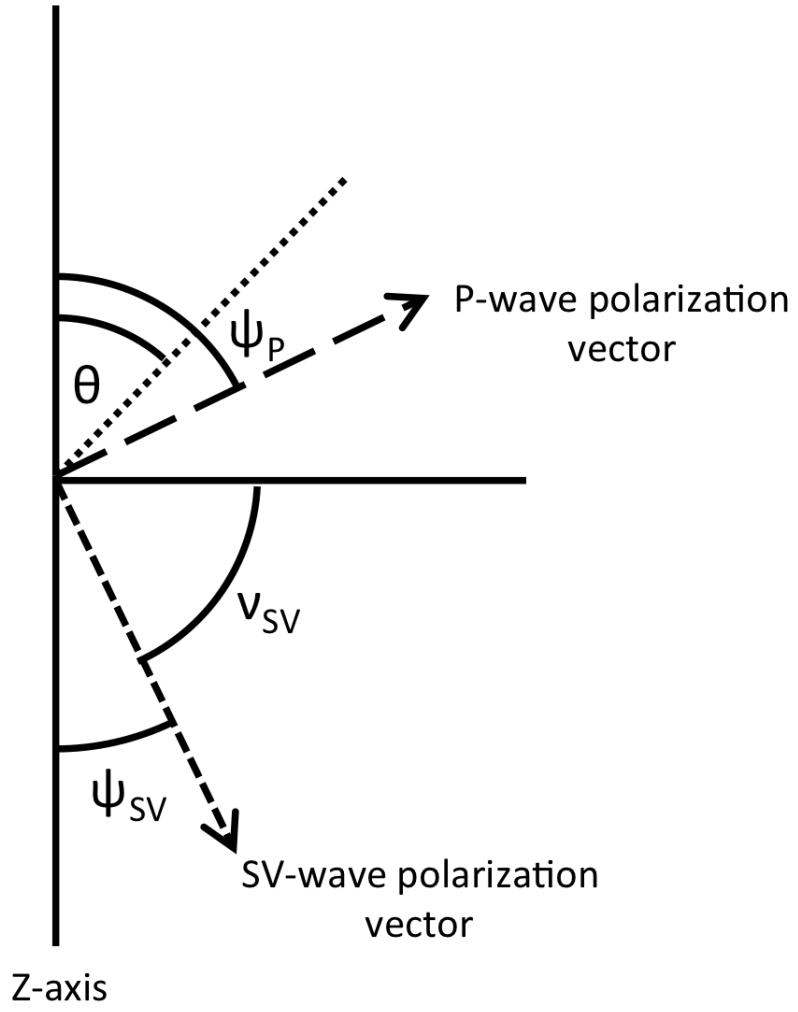

Fig. 13: Diagram of the angles used in the derivation. The phase angle (θ) of both P- and SV-waves, P-wave polarization angle (ψ_P), SV-wave polarization angle (ψ_{SV}), and the angle ν_{SV} between the SV-wave polarization vector and the horizontal.